Experimental measurements of flame structure and time-averaged statistics in turbulent nonpremixed cool flames

Christopher B. Reuter, Omar R. Yehia, Yiguang Ju
Department of Mechanical and Aerospace Engineering, Princeton University
Princeton, NJ, USA

1 Introduction

Fuels possessing two-stage ignition behavior have the capacity to form cool flames [1]. Cool flames are governed by a distinct low-temperature chain-branching chemistry known as peroxy chemistry [2], which involves repeated oxygen additions to large fuel-sized radicals. A critical stabilizing force on the cool flame is the negative temperature coefficient (NTC) effect, in which the chain-branching peroxy chemistry faces increased competition from chain-propagating and chain-terminating pathways as the temperature rises. When there is some kind of loss in the system (thermal and/or radical losses, incomplete combustion via residence time limitations, etc.), the cool flame can be prevented from reaching the second-stage hot flame, resulting in isolated first-stage ignition [3].

Low-temperature chemistry (LTC) and cool flames are quite relevant for existing and future engines, as they are an important factor in ignition in diesel engines [4] and jet engines [5], knock prevention in spark-ignition engines [6], and control of HCCI engines [7]. Since all of these applications occur in turbulent environments, the study of isolated turbulent cool flames can provide valuable insights into the modeling of turbulence-chemistry interactions at low temperatures.

Despite the ubiquity of turbulent combustion in real engines, however, isolated turbulent cool flame experiments have been extremely limited in number. Gökalp et al. [8] studied premixed turbulent cool flames inside a conico-cylindrical reactor. They measured the spectra of temperature fluctuations using hot-wire anemometry in order to infer the influence of combustion on turbulence. Later, stabilized cool flames [9] were used to investigate diesel sprays for fuel reforming applications, but the diagnostics were limited to temperature measurements with thermocouples. Neither of these studies, moreover, explored the structure of turbulent cool flames or gave insight into turbulence-LTC interactions.

To address this, a new Co-flow Axisymmetric Reactor-Assisted Turbulent (CARAT) burner is employed for the study of turbulent nonpremixed cool flames. The turbulent cool flame structure is examined through formaldehyde (CH_2O) planar laser-induced fluorescence (PLIF), acetone PLIF, and Rayleigh scattering. The acetone PLIF images and Rayleigh scattering images are converted into 2-D measurements of mixture fraction and temperature, respectively. The time-averaged conditional statistics are then presented.

Correspondence to: cbreuter@princeton.edu

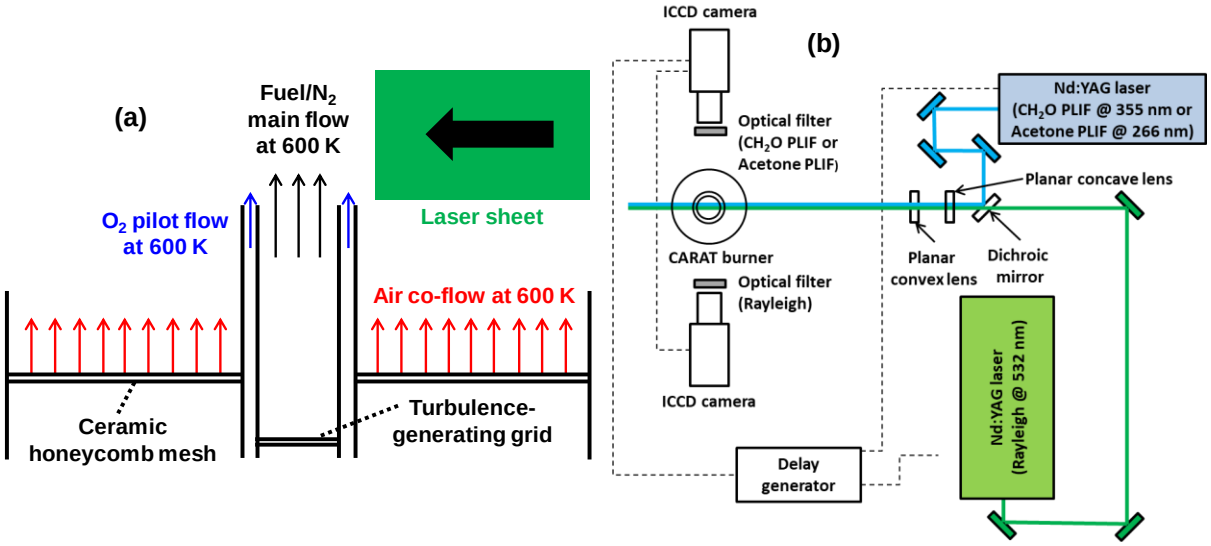

Figure 1. (a) Side view of the CARAT burner, showing the three different flow streams. (b) Top view of the diagnostic setup for the CARAT burner, employing two lasers and two cameras.

2 Experiment

The Co-flow Axisymmetric Reactor-Assisted Turbulent (CARAT) burner, shown in Figure 1a, is a generational upgrade to the Reactor-Assisted Turbulent Slot (RATS) burner of [10] and [11]. The CARAT burner is a Bunsen-type burner with a main exit radius (R) of 7.5 mm. A small annulus (2-mm gap width) surrounding the main exit enables the use of a pilot flow. The CARAT burner also includes a large exterior channel that allows for a heated or vitiated co-flow. The burner has been characterized previously in [12] using hot-wire anemometry. The experimental condition tested in this study is at a main flow velocity of U_{main} = 2.5 m/s, a pilot flow velocity of 1.0 m/s, and a co-flow velocity of 0.50 m/s. All three flows (main, pilot, and co-flow) are set to a temperature of T = 600 K. The main flow contains a mixture of 20% dimethyl ether (DME), 78% nitrogen, and 2% acetone by mole fraction. The pilot flow consists of pure oxygen, and the co-flow is air.

The turbulent cool flame structure is measured through a combination of CH_2O PLIF, acetone PLIF, and planar Rayleigh scattering. Figure 1b depicts the diagnostic setup for the CARAT burner system. The CH_2O PLIF and acetone PLIF rely on the same laser (Quantel Q-smart 850) at different harmonics (3rd and 4th, respectively). The laser used for Rayleigh scattering (Spectra-Physics, lab-170-10) issues a 532 nm beam at an energy of ~400 mJ/pulse. After passing through a dichroic mirror, it joins together with the beam from the second laser, as illustrated in Figure 1b. The two beams are then expanded into sheets 30 mm high and 200 μm thick and positioned over the centerline of the burner. A delay generator controls the timing of both lasers and the CH_2O/acetone ICCD camera. Since the CH_2O/acetone camera can only process images at ~2 Hz (due to readout time limitations), the Rayleigh camera's timing is controlled by the CH_2O/acetone camera to ensure that the images are simultaneous.

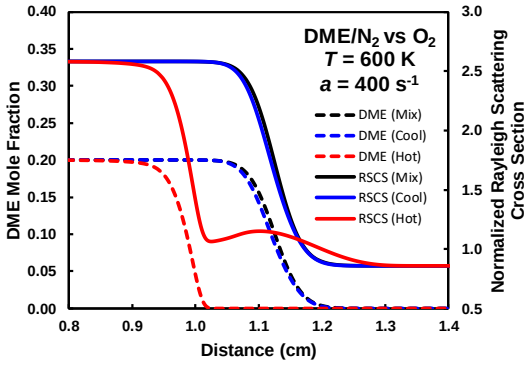

Figure 2. Computed mixture properties for hot flames, cool flames, and unburning mixtures in a laminar nonppremixed counterflow configuration using the Wang kinetic model [14].

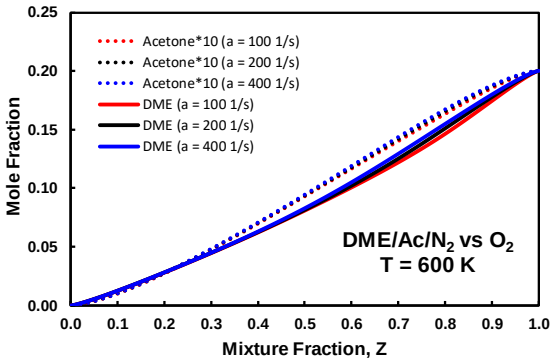

Figure 3. Computed fuel profiles for cool flames at three different strain rates in a laminar nonpremixed counterflow configuration using the Burke kinetic model [16].

3 Data Processing

When 1-D laminar flame calculations are needed, the OPPDIF [13] module of the CHEMKIN package is employed. The kinetic model of Wang et al. [14] is selected for its capability to reproduce the extinction limit of cool flames at 1 atm [15]. However, the Wang model (Figure 2) does not include acetone as a species, so the Burke model [16] is used instead for the DME/acetone laminar flames in Figure 3.

The Rayleigh scattering images (50-100 per run) were processed into temperature measurements in the following manner. First, a few of the Rayleigh scattering images were affected by the presence of residual acetone droplets or dust, so a threshold value of approximately 1.25 times the time-averaged maximum signal was used as a cutoff. The entire run of images was then averaged to obtain a single time-averaged image, and the time-averaged background was subtracted. Next, a correction for the laser power was made to obtain the 2-D images of Rayleigh scattering signal seen in Figure 4a and Figure 4b.

Fortuitously, unlike for hot flames, a cool flame's spatial fuel profile is nearly the same as that of an unburning mixture at the same conditions, as can be seen in the calculations provided in Figure 2. It is also apparent that the calculated Rayleigh scattering cross sections of a cool flame and an unburning mixture (using the values from [17]) are quite similar. Using this premise, dividing the time-averaged Rayleigh scattering signal of the unburning mixture by the time-averaged Rayleigh scattering signal of the cool flame gives the 2-D time-averaged temperature of the cool flame in Figure 4c.

The acetone PLIF images are converted into 2-D mixture fraction fields by simply assuming that a linear relationship exists between the acetone mole fraction and the mixture fraction (Z). As can be seen in Figure 3, this assumption is a sensible one, as a linear fit (with a y-intercept of zero) to the computed acetone mole fraction at a = 400 s^{-1} gives a R^2 value of 0.99. The acetone PLIF images also have the background signal subtracted and are corrected for variations in laser power. Finally, qualitative 2-D images of CH_2O signal are derived from the CH_2O PLIF through the same sequence of background subtraction followed by laser power correction.

4 Results and Discussion

Figure 5a shows a representative instantaneous CH_2O PLIF image of a DME turbulent nonpremixed cool flame for the U_{main} = 2.5 m/s case. The turbulent cool flame is clearly corrugated but unbroken, with the majority of the wrinkling occurring on the fuel side of the flame. In a few images, pockets of unburned reactants or flame islands are visible. The higher likelihood of fuel-side fluctuations is confirmed quantitatively by the large values of the root mean square (RMS) of the CH_2O PLIF signal in Figure 5c. This is due to the presence of the turbulent grids upstream of the DME/N_2/acetone main flow.

The instantaneous, mean (time-average), and RMS of the 2-D mixture fraction field, obtained from the acetone PLIF measurements, can be seen in Figure 6. As mentioned previously, the acetone mole fraction linearly correlates quite well with the mixture fraction; however, it was difficult to achieve exactly $Z = 1$ due to the inherent variations in the experimental PLIF signal. Therefore, it is estimated that an uncertainty in mixture fraction of approximately ±10% is present. The stoichiometric mixture fraction (Z_{stoich} = 0.622) of the time-averaged image is indicated by the dotted black lines. It is evident from Figure 6b that Z_{stoich} lies within $-1 < r/R < 1$ over this range of heights above the burner. The maximum RMS fluctuations in mixture fraction shown in Figure 6c are also centered around $r/R = \pm 1$.

Similarly, the 2-D measurements of Rayleigh scattering signal are split into instantaneous, time-averaged, and RMS images in Figure 7. The use of simultaneous acetone PLIF and Rayleigh scattering measurements is apparent when comparing the images of instantaneous mixture fraction in Figure 6a and instantaneous Rayleigh scattering signal in Figure 7a. Additionally, like the RMS fluctuations in mixture fraction, the RMS values of the Rayleigh scattering signal in Figure 7c peak in the vicinity of $r/R = \pm 1$. Note that the locally high RMS values in the upper left and upper right corners are due to the presence of dust particles.

As mentioned previously, time-averaged measurements of the cool flame temperature (Figure 4c) are obtained through the time-averaged Rayleigh scattering signal of the cool flame along with the time-averaged Rayleigh scattering signal of an unburning mixture baseline case. The 2-D spatial measurements

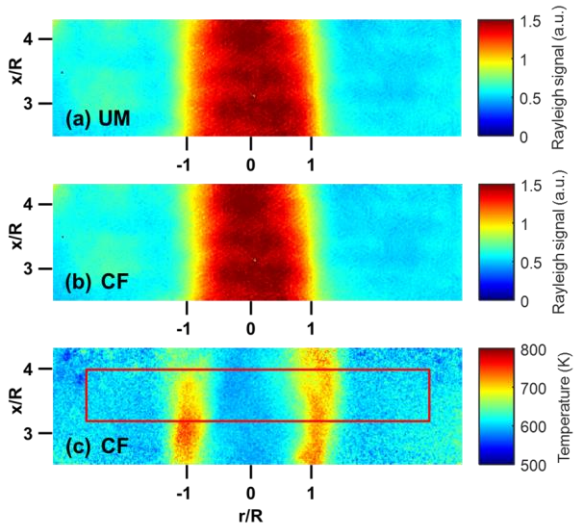

Figure 4. Time-averaged (a) Rayleigh scattering signal from an unburning mixture, (b) Rayleigh scattering signal from a cool flame, and (c) temperature for a cool flame. The red box indicates where the conditional statistics are derived.

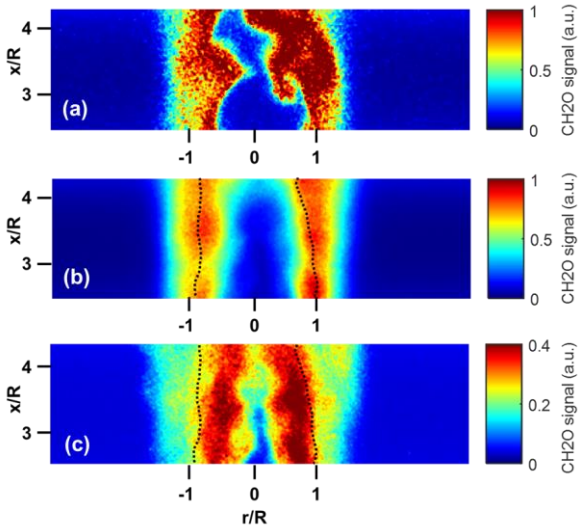

Figure 5. (a) Instantaneous CH_2O PLIF signal, (b) time-averaged CH_2O PLIF signal, and (c) root mean square (RMS) of CH_2O PLIF signal. The dotted lines indicate the time-averaged stoichiometric mixture fraction (Z_{stoich}).

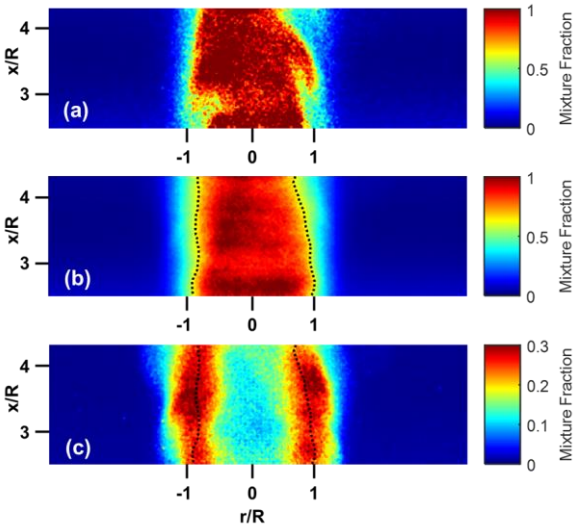

Figure 6. (a) Instantaneous mixture fraction image, (b) time-averaged mixture fraction, and (c) root mean square (RMS) of mixture fraction. The dotted lines indicate the time-averaged Z_{stoich}.

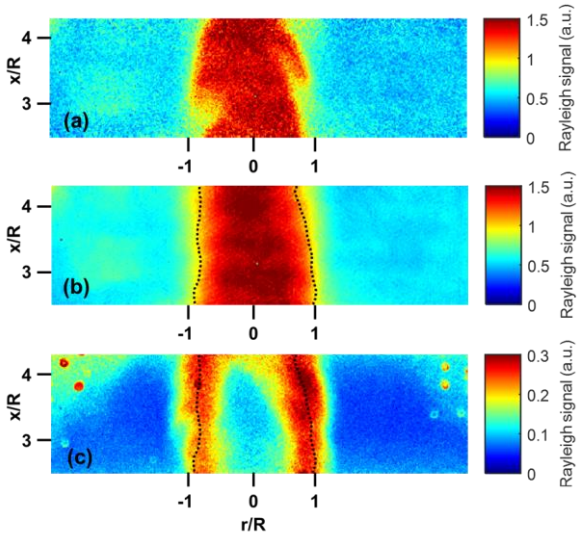

Figure 7. (a) Instantaneous Rayleigh scattering signal, (b) time-averaged Rayleigh scattering signal, and (c) RMS of the Rayleigh scattering signal. The dotted lines indicate the time-averaged Z_{stoich}.

of temperature and mixture fraction are then converted into conditional statistics through the following process. Since each point (pixel) in the 2-D spatial plots has both a time-averaged temperature and a time-averaged mixture fraction, a scatterplot of mixture fraction versus temperature can be created (i.e., the grey dots in Figure 8). The temperatures within bins of $\Delta Z = 0.02$ are then averaged to find the time-averaged temperature conditioned on mixture fraction (i.e., the black circles in Figure 8). Note that all conditional statistics are limited to the red box within Figure 4c.

An immediately obvious aspect of Figure 8 is that the maximum flame temperature (T_{max}) is located on the lean side of Z_{stoich}. One unusual trait of cool flames is the crossing of Z_{stoich} by T_{max} as the strain rate changes without any other modifications in the boundary conditions. The black line in Figure 9 shows this occurring for computed nonpremixed laminar cool flames with $X_{DME} = 0.2$ and $X_{N2} = 0.8$ on the fuel side and $X_{O2} =$

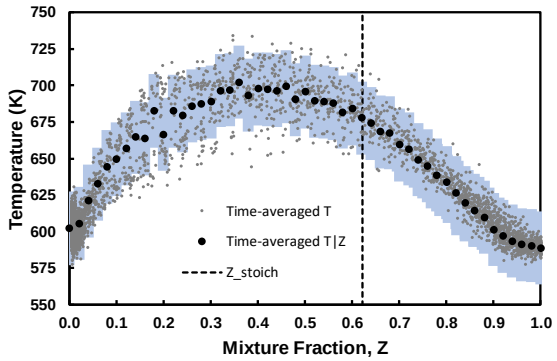

Figure 8. Time-averaged temperature versus mixture fraction. Large circles show the conditional average (error bars included); small circles show the scatter.

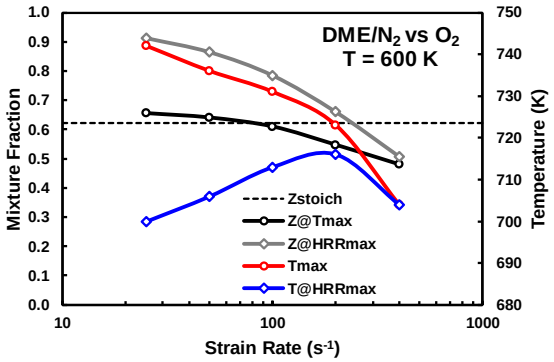

Figure 9. Computed maximum temperatures and heat release rates for a range of strain rates in a laminar nonpremixed counterflow configuration using the Wang model [11].

1.0 on the oxidizer side. T_{max} is located on the rich side of Z_{stoich} for low strain rates (25-50 s^{-1}) but on the lean side of Z_{stoich} for high strain rates (200-400 s^{-1}). The reason for this is explained below.

First, it is clear that T_{max} (red line in Figure 9) decreases with increasing strain rate. Another observation is that the mixture fraction at HRR_{max} (grey line) is always richer than the mixture fraction at T_{max} (black line). But perhaps the most important factor contributing to the crossing of Z_{stoich} is that the temperature at HRR_{max} (blue line) is constrained between 700 K and 720 K. This is due to the confluence of available DME, O_2, OH, and CH_3OCH_2 for high heat release reactions ($CH_3OCH_2 + O_2 = CH_3OCH_2O_2$ and $CH_3OCH_3 + OH = CH_3OCH_2 + H_2O$ are the two highest heat production reactions in DME nonpremixed cool flames [15]).

A likely reason for T_{max} and especially HRR_{max} peaking on the rich side of Z_{stoich} for low strain rates is the nature of the low-temperature peroxy chain-branching sequence. Only two O_2 additions to DME are required for low-temperature chain branching; consequently, at low strain rates (i.e., high residence times), DME has plenty of time to react before reaching Z_{stoich}. However, for the highest strain rate of a = 400 s^{-1} (the lowest residence time), most of the DME does not react until it is already on the lean side of Z_{stoich}. Therefore, the crossing of Z_{stoich} by T_{max} is caused by the significant fuel and oxidizer leakage across Z_{stoich}. An alternative way of thinking about this is in terms of the activation energy—nonpremixed hot flames have large activation energies and are therefore much more temperature-dependent than residence time-dependent, but nonpremixed cool flames with lower activation energies experience competition between the two. Therefore, the location of nonpremixed hot flames tends to be very close to Z_{stoich}, whereas the location of nonpremixed cool flames can be a strong function of the strain rate (residence time).

5 Conclusion

Turbulent nonpremixed DME cool flames have been studied through CH_2O PLIF, acetone PLIF, and planar Rayleigh scattering. Two-dimensional mixture fraction and temperature measurements have been derived from the acetone PLIF and Rayleigh scattering signals, respectively. Due to the presence of the turbulent grids in the main flow, the RMS fluctuations in the turbulent cool flame's CH_2O PLIF signal occur predominantly on the fuel side of the flame, and the flame displays substantial wrinkling. The similarities between cool flames and unburning mixtures allow for quantitative temperature measurements without the need for maintaining constant Rayleigh scattering cross sections. For the experimental condition reported, the time-averaged temperature peaks on the lean side of the stoichiometric mixture fraction. The results of this experimental investigation give much-needed insight into the interactions between cool flames and turbulence.

References

[1] H.J. Curran, P. Gaffuri, W.J. Pitz, C.K. Westbrook, A comprehensive modeling study of n-heptane oxidation, Combust. Flame 114 (1998) 149-177.
[2] J. Zádor, C.A. Taatjes, R.X. Fernandes, Kinetics of elementary reactions in low-temperature autoignition chemistry, Prog. Energy Combust. Sci. 37 (2011) 371-421.
[3] C.B. Reuter, S.H. Won, Y. Ju, Experimental study of the dynamics and structure of self-sustaining premixed cool flames using a counterflow burner, Combust. Flame 166 (2016) 125-132.
[4] S.A. Skeen, J. Manin, and L.M. Pickett, Simultaneous formaldehyde PLIF and high-speed schlieren imaging for ignition visualization in high-pressure spray flames, Proc. Combust. Inst. 35 (2015) 3167-3174.
[5] A. Burkert, W. Paa, Ignition delay times of single kerosene droplets based on formaldehyde LIF detection, Fuel 167 (2016) 271-279.

[6] A. Fish, I.A. Read, W.S. Affleck, W.W. Haskell, The controlling role of cool flames in two-stage ignition, Combust. Flame 13 (1969) 39-49.
[7] H. Yamada, K. Suzaki, A. Tezaki, Y. Goto, Transition from cool flame to thermal flame in compression ignition process, Combust. Flame 154 (2008) 248-258
[8] I. Gökalp, G.M.L. Dumas, R.I. Ben-Aïm, Temperature field measurements in a premixed turbulent cool flame, Symp. (Int.) Combust. 18 (1981) 969-976.
[9] D.I. Kolaitis, M.A. Founti, A tabulated chemistry approach for numerical modeling of diesel spray evaporation in a "stabilized cool flame" environment, Combust. Flame 145 (2006) 259-271.
[10] S.H. Won, B. Windom, B. Jiang, Y. Ju, The role of low temperature fuel chemistry on turbulent flame propagation, Combust. Flame 161 (2014) 475-483.
[11] B. Windom, S.H. Won, C.B. Reuter, B. Jiang, Y. Ju, S. Hammack, T. Ombrello, C. Carter, Study of ignition chemistry on turbulent premixed flames of n-heptane/air by using a reactor assisted turbulent slot burner, Combust. Flame 169 (2016) 19-29.
[12] C.B. Reuter, O. Yehia, S.H. Won, M. Fu, K. Kokmanian, M. Hultmark, Y. Ju, Experimental Investigation of the Stabilization and Structure of Turbulent Cool Diffusion Flames, 56th AIAA Aero. Sci. Meeting, Kissimmee, FL (2018).
[13] A.E. Lutz, R.J. Kee, J.F. Grcar, F.M. Rupley, OPPDIF: A Fortran program for computing opposed-flow diffusion flames, Sandia National Laboratories Report SAND96-8243, 1997.
[14] Z. Wang, X. Zhang, L. Xing, L. Zhang, F. Herrmann, K. Moshammer, F. Qi, K. Kohse-Höinghaus, Experimental and kinetic modeling study of the low- and intermediate-temperature oxidation of dimethyl ether, Combust. Flame 162 (2015) 1113-1125.
[15] C.B. Reuter, R. Zhang, O.R. Yehia, Y. Rezgui, Y. Ju, Counterflow flame experiments and chemical kinetic modeling of dimethyl ether/methane mixtures, Combust. Flame 196 (2018) 1-10.
[16] U. Burke, K.P. Somers, P. O'Toole, C.M. Zinner, N. Marquet, G. Bourque, E.L. Petersen, W.K. Metcalfe, Z. Serinyel, H.J. Curran, An ignition delay and kinetic modeling study of methane, dimethyl ether, and their mixtures at high pressures, Combust. Flame 162 (2015) 315-330.
[17] F. Fuest, R.S. Barlow, J.-Y. Chen, A. Dreizler, Raman/Rayleigh scattering and CO-LIF measurements in laminar and turbulent jet flames of dimethyl ether, Combust. Flame 159 (2012) 2533-2562.